Iranian Journal of Science and Technology, Transactions of Mechanical Engineering (2023) 47:809–828
https://doi.org/10.1007/s40997-022-00551-8

RESEARCH PAPER

The Hydrodynamic Challenge of Initial to Sheet/Cloud Cavitating Flow Around ClarkY11.7% Hydrofoil Using Recent Turbulence and Cavitation Models

Maryam Saberinia[1] · **Mahmoud Pasandidehfard**[1]

Received: 28 September 2020 / Accepted: 16 October 2022 / Published online: 2 November 2022

Abstract
It is crucial to predict accurately the onset of cavitation and somewhat after that as one of the fluid flow hydrodynamics limitations. In the present study, four cavitation models inclusive of Singhal, Zwart, Kunz, Sauer, and also three recent improved RANS turbulence models including *k-kl-ω*, SST *k-ω*, and SST transition are examined for initial to cloud cavitation flows. Hence, the cavitating flow over a two-dimensional ClarkY11.7% hydrofoil at angles of attack 8 and 10 degrees and Reynolds number of 8×10^5 is numerically studied by means of ANSYS-Fluent, and the results are compared against experimental data in a range of cavitation numbers of (0.8–4). It has been tried a great deal, to increase the accuracy of all implemented methods and techniques. Comparisons show that the numerical predictions could be improved considerably. In particular, we report that using the combination of Zwart cavitation and transient $k-kl-\omega$ turbulence models leads to much better agreement with experimental results for these conditions of flow. Further, the unsteady flow dynamics and pressure variations of different points on the hydrofoil against time have been illustrated.

Keywords Turbulence models · Cavitation models · Initial cavitation · ClarkY11.7%

1 Introduction

Liquids vaporize through two ways; In one way, temperature increases at constant pressure, and in the other way, due to increasing velocity, pressure drops below the vapor pressure and leads to cavitation (Movahedian et al. 2019). Cavitation is a common occurrence in hydraulic systems such as turbines, pumps, piping systems, fuel injectors, submarines, underwater vehicles, marine propeller blades, and hydrofoils (Pendar and Roohi 2018).

Cavitation is generally known as an unfavorable phenomenon and has undesirable effects like noise, erosion, vibration, efficiency issues, and hydraulic losses (Wang et al. 2019). Cavitating flows are highly unsteady, turbulent, multiphase, nonlinear, and oscillating. Else ways, the unpleasant effects of cavitation are intentionally used to modify and improve the surface or mechanical properties, for example, cleaning, cutting, or peening with low energy consumption (Hutli et al. 2019). Numerical simulation of these flows is accompanied by some difficulties due to complex interactions and large variations of density between the liquid and vapor phases (Wu and Chen 2016; Hejranfar et al. 2015).

Cavitation number is a dimensionless number used to determine the sensitivity of flow to cavitation and to characterize cavitating flows. It is defined as $\sigma = \frac{P-P_v}{0.5\rho_l U^2}$ where P and U are, respectively, the pressure and velocity of free-stream flow,P_v is the vapor pressure, and ρ_l is the liquid density. This number represents the ratio of the difference between a free stream and inside of the cavity pressure energies to the kinetic energy of the free stream (Erfanian and Anbarsooz 2018; Štigler and Svozil 2009). Based on the reduction of cavitation number, cavitating flows are categorized into four regimes: inception cavitation, sheet cavitation, cloud cavitation, and supercavitation (Wang et al. 2001). Obvious limitations of the measurement techniques, fast-track development and broad application of powerful computers, the ability of time-saving, and economic aspects caused propagation and popularity of the numerical methods in the last few years (Bensow and Bark 2010; Huang et al. 2010; Park and Rhee 2012; Palau Salvador and Frankel

✉ Mahmoud Pasandidehfard
fard_m@um.ac.ir

[1] Ferdowsi University of Mashhad, Mashhad, Iran

2004; Wienken et al. 2006). Depending on the physics of the problem, numerical simulations of cavitation can be carried out by two theories: interface tracking methods and interface capturing methods. In the first theory, the cavity pressure is assumed to be constant and equal to the saturated vapor pressure. Thus, the phase's interface acts as a boundary, and the calculations are done just for the liquid phase.

The interface tracking methods are limited to stable sheet cavitation and are not suitable for predicting cavitation in the cases with growth and detachment of the bubbles or 3D interface tracking (Hejranfar et al. 2015; Wang et al. 2001). This method works in two ways: (1) Using potential flow Eqs. (2) Using Euler and Navier–Stokes equations (Hejranfar and Hajihassanpour 2017). Notwithstanding the first category, in the interface capturing methods, flow is presumed to be a two-phase, single fluid with a mixture density. The density of the mixture contiguously alters among liquid and vapor in this method, and it is assumed to be there is no slip velocity between phases (Hejranfar et al. 2015; Hejranfar and Hajihassanpour 2017; Passandideh-Fard and Roohi 2008; Roohi et al. 2013).

The main difference between the models of this category lies in the various definitions of the density field. One common approach to determining the density is to use the barotropic model. Delannoy and Kueny proposed this model in 1990 and established a direct correlation between density and pressure through an equation of state (Delannoy 1990).

The most challenging part of this model is how to specify a proper equation of state which is compatible with the nature of the problem. It needs enough experimental data in every case (Roohi et al. 2013). Different state laws are suggested and applied by many researchers in the literature (Reboud et al. 1998, 2003; Goncalves and Patella 2009; Goncalvès and Patella 2011; Goncalvès 2013; Dular and Coutier-Delgosha 2009; Iga et al. 2003; Song 1998; Shin and Ikohagi 1999; Ventikos and Tzabiras 2000; Qin et al. 2003; Coutier-Delgosha et al. 2005, 2002, 2007, 2003a).

The barotropic model presumes a complete thermodynamic and mechanical equilibrium between phases among the evaporation and condensation; Hence, this model does not include flow details such as the mass exchange and heat transfer (Goncalvès 2013; Koop and Hoeijmakers 2008; Liuzzi 2012; Niu et al. 2007; Causon and Mingham 2013; Saurel et al. 1999). Moreover, the pressure and density gradients are always parallel in the barotropic models, and baroclinic torque is zero accordingly. The vorticity production that is the outcome of baroclinic torque and one of the most important aspects of cavitating flows is neglected in this model. Consequently, barotropic models can not accurately predict the dynamics of the cavitating flows (Gopalan and Katz 2000; Senocak and Shyy 2002). Another meticulous and prevalent approach is the transport equation-based model (TEM) which solves an additional transfer equation including source terms for mass/volume fraction of vapor or liquid phase and estimation of density (Hong et al. 2017; Zhou et al. 2019). Due to the convective character of the advection equation, TEM models can consider inertial forces and detachment of cavity bubbles (Wang et al. 2001). There are some cavitation models with different transport equations in the literature. Kubota model is derived from the Rayleigh–Plesset equation with the assumption of constant nuclei density. Rayleigh–Plesset equation shows how alters the radius of the spherical bubbles in incompressible fluid (Cheng et al. 2020). In this model, the source terms are proportional to the square root of local pressure and vapor pressure difference (Kubota et al. 1992). Based on the semi-analytical relations and using artificial compressibility, Merkle (1998) proposed a mass transfer model that contains both mass and volume fractions. Source terms of the Merkle model are directly related to the pressure difference and include the time scale factor. Sauer (2001) and Yuan (2001) suggested a model based on the Rayleigh–Plesset equation that is independent of the empirical constants. Kunz (2000) established a model with a preconditioning algorithm and source terms based on dimensional arguments and experimental observations. The presented model by Singhal (2002) named the full cavitation model, is derived from a reduced form of the Rayleigh–Plesset equation for bubble dynamics and magnitude of non-condensable gases. Senocak and Shyy (2004a, 2004b) recommended a completely analytical model using transport laws across boundaries and developed an interfacial dynamic-based model (IDM). In their model, the effect of empirical constants is eliminated and replaced with explicit calculations. The Zwart (2004) model comes from the simplified Rayleigh–Plesset equation for bubble dynamics. The crucial assumption in the derivation of this model is that all of the system bubbles have the same size, and there is no interaction between them. This model has two parts, one for condensation and the other for evaporation, where the nucleation site of volume fraction (r_{nuc}) is introduced into vaporization expression. Despite applying, modifying, and developing mentioned models in many pieces of research, there are a few comparative studies between different cavitation models. It is due to the complexity of the cavitating flows, particularly in the sheet to cloud regimes. Frikha et al. (2008) compared different cavitation models and observed resemblances between them. Morgut et al. (2011) calibrated disparate cavitation models by adjusting the empirical coefficients using optimization strategy and compared the capability of these models in the prediction of sheet cavitation. In their study, the results of various models are similar if appropriate regulation is conducted. Ducoin et al. (2012) concluded that the Merkle model has more stability than the Singhal and Kubota models, especially in the unsteady cavitating flows. Tran et al. (2015), showed that in the simulation of stable sheet/cloud cavitation, the Merkle model has

a better performance than the Kubota model and gives more information about the dynamic behavior of the fluid flow. Capurso et al. (2017) recommended the Zwart cavitation model to study of sheet cavitation regime. Yu et al. (2019) compared three widespread cavitation models. Their study indicates that under different conditions, every model can have a good result.

Furthermore, the selection of a proper turbulence model is one of the important matters, because cavitating flows are usually highly unsteady and occur in high Reynolds numbers that makes them sophisticated subjects. Different approaches have been applied to simulate cavitation and an ordinary technique is to solve Reynolds-averaged Navier–Stokes (RANS) equations. The equations of these turbulence models are derived from non-cavitating flow, thus, an eddy viscosity model is added for considering cavitation effects (Liu et al. 2013; Coussirat et al. 2016a, 2016b; Decaix and Goncalves 2012). More progressive turbulence models are Reynolds stress model (RSM), the large eddy simulation model (LES), direct numerical simulation (DNS), and detached eddy simulation (DES). Although the LES and DES models have supremacy over the RANS models in terms of accuracy and providing more particular details of interactions that happen in the cavitating flow, they are too costly due to the greater mesh size and longer simulation time periods, making them relatively impracticable in the industrial context. Hence, it is not common to use these models in engineering and industrial applications whenever general information of flow is needed (Corson et al. 2009; Salim et al. 2011; Liu et al. 2014; Gosman 1999). Nevertheless, some of the recent investigations of cavitating flows that used the LES model are reviewed as following. The anisotropic minimum dissipation (AMD) model as a static type of sub-grid scale (SGS) novel models in the LES simulation approach has been used in references (LarKermani et al. 2018; Zahiri and Roohi 2019, 2021). Pasandideh-Fard and Roohi (2008) performed a two-dimensional axisymmetric simulation of cavitating flows and developed a numerical model using a modified Volume-of-Fluid (VOF) technique. They tried the developed model over different geometries in a wide range of cavitation numbers and the good accuracy of this numerical method in the prediction of cavity shapes and cavity closure region was concluded. Roohi et al. (2013) used the LES turbulence model in companion with the VOF capturing technique to simulate the unsteady cloud cavitation and the steady supercavitation over a 2D ClarkY11.7% hydrofoil. They evaluated the performance of Kunz and Sauer cavitation models and it has been revealed that using the LES and VOF models with Kunz or Sauer mass transfer models provides an accurate prediction of the cavity characteristics. The results obtained from the Kunz cavitation model indicated a good agreement between the experimental data and numerical simulations of the cavity diameter, lift and drag coefficients. Authors of reference (Roohi et al. 2016) compared different turbulence and mass transfer models in terms of the unsteady cavitating flow and supercavitation simulation behind a 3D disk using the VOF tracking method. The LES turbulence model and Kunz cavitation model calculated the cavity length and drag coefficient more precisely than the other models, while the combination of the Sauer mass transfer model and the LES model presented better results for cavity diameter approximation. A three-dimensional simulation of the unsteady cavitation and supercavitation around a hemispherical headform body and a conical cavitator was carried out by Pendar et al. (2016). They compared various turbulence and cavitation models using the VOF tracking technique and it was found the different combinations of these models had similar results of the general cavitation characteristics like the cavity length, but the boundary layer separation and re-entrant jet prediction of the various models were different. In another work, Pendar et al. (2018) simulated the partial cavitation and supercavitation over a sphere using the LES turbulence model and VOF method in combination with Sauer mass transfer model and compared the results with those of the non-cavitating flow at the same Reynolds number. According to their results, cavitation suppresses the flow instabilities in the near wake region and delays the three-dimensional vortices breakdown. Kolahan et al. (2019) performed a 3D numerical wavelet analysis of cavitating flow over a sphere in a range of cavitation numbers utilizing the LES turbulence and Sauer cavitation models. They showed the flow fluctuations enhance by increasing the cavitation number. Movahedian et al. (2019) employed the LES turbulence model, Kunz mass transfer model, and VOF method to conduct a 3D numerical simulation of unsteady cavitation around a twisted NACA16012 hydrofoil. The findings were representative of the horseshoe vortexes growth with decreasing the cavitation number. They also indicated the side-entrant jets and the radially diverged re-entrant jet at the end of the cavity attributed by the twisted form of the hydrofoil. Pendar et al. (2020) performed a 3D numerical simulation of cavitation around a wavy leading edge (WLE) hydrofoil and compared the results with a straight leading edge (SLE) hydrofoil and employed the LES model and VOF method to investigate the cavitating flow characteristics. The findings showed that the laminar separation bubble was developed on the suction side of the WLE hydrofoil and as a result it impedes the considerable flow separations. In addition, the WLE hydrofoils depicted a considerable reduced level of unsteady fluctuations at the periodic vortex shedding frequency.

However, from all of the above-mentioned papers it is obvious that using the LES model needs significantly more time to simulate the practical applications. As for most cases, we must wait more than one month for one running answer with conventional computer systems. Therefore, RANS models become popular because of their convenient

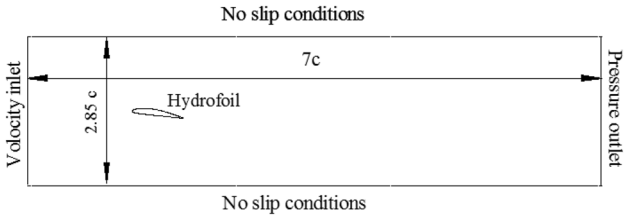

Fig. 1 Computational domain and boundary conditions

Table 1 Flow and boundary conditions

Inlet constant velocity (m/s)	8	
Vapor pressure (pa)	3540	
Density (kg/m^3)	Liquid	998.2
	Vapor	0.5543
Dynamic viscosity$(kg/m.s)$	Liquid	0.001003
	Vapor	1.34×10^{-5}

Table 2 Grids information for sensitivity study

Mesh No	Number of nodes on hydrofoil	Number of cells
Grid-1	560	154,000
Grid-2	640	167,400
Grid-3	720	180,600
Grid-4	800	193,800

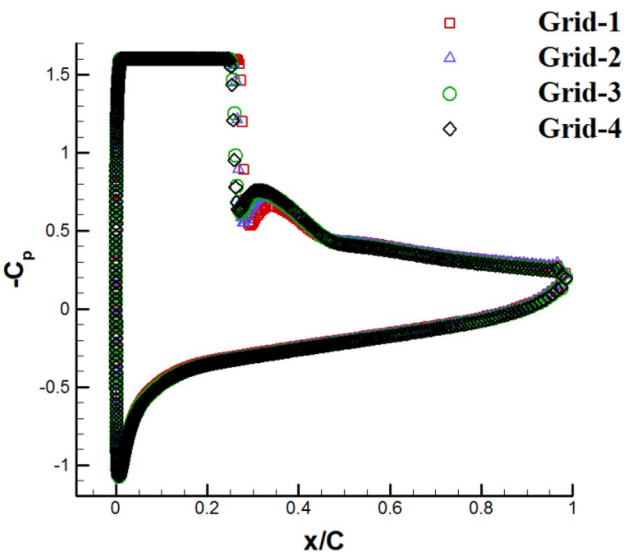

Fig. 2 Averaged pressure coefficient of different grids at $\sigma = 1.6$

accuracy in a wide range of turbulent flows and rational computation expenses (Zhang et al. 2016; Lu et al. 2012). Coutier-Delgosha et al. (2003b) compared four turbulence models for simulating unsteady cavitation in a Venturi-type section. They concluded that the modified $k-\varepsilon RNG$ and $k-\omega$ models with compressibility effects were more consistent with the experiments. The result of Goncalvès et al. (2011) studies states that $SSTk-\omega$ model is more precise than the other RANS models in the case of Venturi geometries. Yin et al. (2018) compared the capability of four turbulence models in predicting the unsteady cavitating flow around a twisted hydrofoil. The results governed by $SSTk-\omega$ model are in better agreement with experimental data. According to Geng et al. (2020) research, $SSTk-\omega$ performs better than $k-\varepsilon$ model for cavitating flows.

The literature shows that the flow at initial cavitation and sheet/cloud cavitation areas need to pay more attention to and most of the simulations that have been reported till now; do not show satisfactory predictions, particularly for initial to sheet/cloud cavitation. At the initial cavitation stage, lift coefficient increases at first and then decreases suddenly with reducing the cavitation number. The unsteadiness of cloud cavitation is also the other challenge for the cavitation and turbulence models. The main objective of this study is to investigate the performance of prevalent cavitation models and the accuracy of different turbulence models in the prediction of cavitating flows around ClarkY11.7% hydrofoil for the range of initial to cloud cavitation numbers. Our numerical results in terms of lift and drag coefficients, cavity length, and its shape comparing the experimental data have been presented for a broad range of cavitation numbers. Further, applying higher order of techniques, an appropriate combination of cavitation, and turbulence models are explored to improve the predictions at the initial cavitation stage.

2 Boundary Conditions and Computational Setup

A 2D ClarkY11.7% hydrofoil with angles of attack (AOA) equal to 8° and 10° is studied in this paper. Figure 1 shows the computational domain and boundary conditions. The domain size is 700 mm × 285 mm and its length extends two times of chord lengths ahead of the leading edge and four times of chord lengths behind the trailing edge. The hydrofoil is placed at the middle of the domain's width, and its chord length is $c = 100$ mm. Table 1 gives the flow and boundary conditions. The structured quadrate meshes have been enforced as the geometry of ClarkY11.7% is not so complex. Four grids with different sizes are inspected to study the impact of mesh quality influence on the cavity length. The number of cells and cavity length of each grid are reported in Table 2 and averaged pressure coefficients of these grids are compared in Fig. 2. This figure depicts that the pressure coefficients of these grids are nearly close

together and there is a slight difference between the third and fourth grids. Therefore, we chose to use Grid-3 for the upcoming simulations. Figure 3 illustrates the mesh around the ClarkY11.7% hydrofoil and close-up views along leading and trailing edges. The mesh around the leading edge is more concentrated than the trailing edge. Therefore, this mesh is fine enough to satisfy $y^+ < 1$ everywhere near the hydrofoil wall as shown in Fig. 4. Figure 5 depicts the hydrofoil pressure coefficient in non-cavitating flow compared to measured data (Matsunari et al. 2012). A good agreement between simulation and experiments can be seen. In order to resolve the real transient evolution of cavitating flow, the time step is set as 6.25×10^{-5} s, which is equivalent to t_{ref} /200 (t_{ref}= c/U_∞ where U_∞ is the free-stream velocity at the inlet), as suggested by Coutier-Delgosha et al. (2003a).

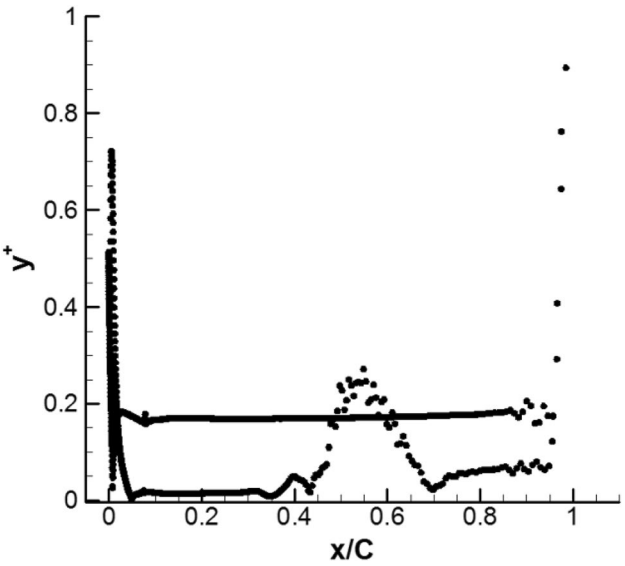

Fig. 4 y^+ value close to the hydrofoil surface

3 Mathematical Model

In this study, the multiphase flow composed of vapor and liquid phases is assumed to be incompressible and homogeneous in that the phases have the same velocity and

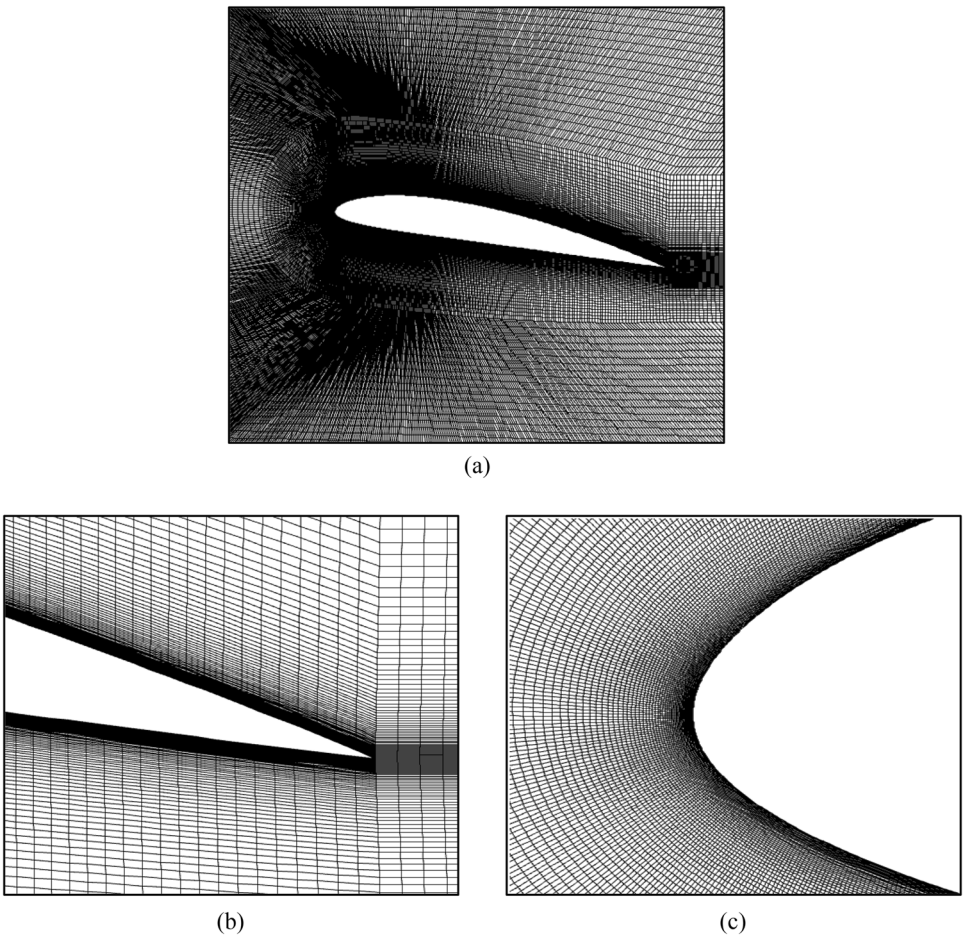

Fig. 3 **a** Structured mesh around ClarkY11.7% hydrofoil at angle of attack 8°, **b** trailing edge close view, and **c** leading edge close view

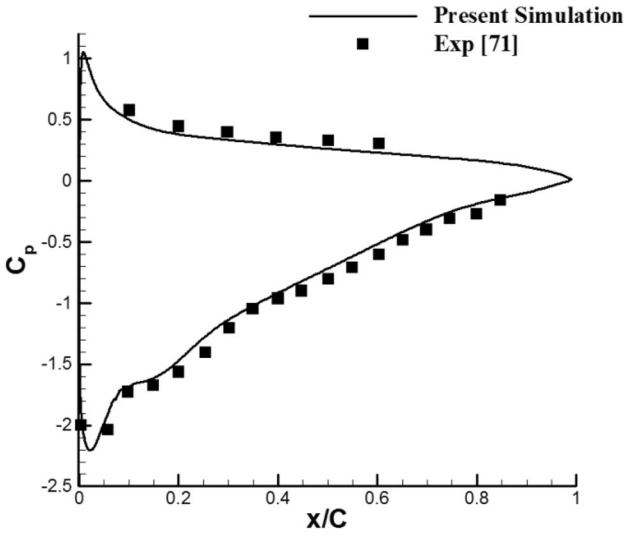

Fig. 5 Pressure coefficient distribution along the hydrofoil for non-cavitating conditions

pressure. Then, the governing equations for the mixture fluid are presented by the following expressions.

Continuity and momentum equations are:

$$\frac{\partial \rho_m}{\partial t} + \frac{\partial}{\partial x_j}\left(\rho_m u_j\right) = 0 \tag{1}$$

$$\frac{\partial(\rho_m u_i)}{\partial t} + \frac{\partial}{\partial x_j}\left(\rho_m u_i u_j\right) = -\frac{\partial P}{\partial x_i} + \frac{\partial}{\partial x_j}\left(\mu_m \frac{\partial u_i}{\partial x_j}\right) \tag{2}$$

where u is velocity, P is pressure, ρ_m and μ_m are mixture density and dynamic viscosity, respectively. The (i,j,k) subscripts signify directions in the Cartesian coordinates.

$$\rho_m = \rho_v \alpha_v + (1-\alpha_v)\rho_l \tag{3}$$

$$\mu_m = \mu_v \alpha_v + \left(1-\alpha_v\right)\mu_l. \tag{4}$$

α_v is the vapor volume fraction. Respectively, ρ_v and ρ_l are the vapor and liquid density, μ_v and μ_l are the vapor and liquid dynamic viscosity.

Equation (5) represents vapor transport equation:

$$\frac{\partial \rho_v \alpha_v}{\partial t} + \frac{\partial}{\partial x_j}\left(\rho_v \alpha_v u_j\right) = \dot{m}^+ + \dot{m}^- \tag{5}$$

where $\dot{m}^+$ and $\dot{m}^-$, respectively, are the mass transfer source terms during evaporation and condensation.

In the following section, we briefly describe four propounded cavitation models in this study.

4 Mass Transfer Models

4.1 Singhal Cavitation Model

This model is suggested by Singhal (2002) and because it takes into account all the first-order effects, named the "full cavitation model." The mass source terms of this model state as follows**:**

$$\dot{m}^+ = C_e \frac{\sqrt{k}}{T}\rho_l \rho_v \left(\frac{2}{3}\frac{P_v - P}{\rho_l}\right)^{\frac{1}{2}}\left(1-f_v\right) if P \le P_v \tag{6}$$

$$\dot{m}^+ = C_c \frac{\sqrt{k}}{T}\rho_l \rho_v \left(\frac{2}{3}\frac{P - P_v}{\rho_l}\right)^{\frac{1}{2}} f_v if P_v \le P. \tag{7}$$

In the above equations, k is the turbulent kinetic energy, T is the surface tension, f_v is the vapor mass fraction, P_v is the vapor pressure and empirical constants C_e and C_c are adjusted to 0.02 and 0.01, respectively**.**

4.2 Sauer Cavitation Model

Another exerted model in this simulation is the Schnerr and Sauer (2001) model which its equations are as follows:

$$\dot{m}^+ = \frac{\rho_l \rho_v}{\rho}\alpha_v\left(1-\alpha_v\right)\frac{3}{R_B}\left(\frac{2}{3}\frac{P_v - P}{\rho_l}\right)^{\frac{1}{2}} if\ P \le P_v \tag{8}$$

$$\dot{m}^+ = \frac{\rho_l \rho_v}{\rho}\alpha_v\left(1-\alpha_v\right)\frac{3}{R_B}\left(\frac{2}{3}\frac{P - P_v}{\rho_l}\right)^{\frac{1}{2}} if\ P_v \le P \tag{9}$$

where R_B is the bubble radius given by $R_B = \frac{\alpha}{1-\alpha}\frac{3}{4\pi n}$. n is number of bubbles**.**

4.3 Zwart Cavitation Model

The Zwart (2004) cavitation model is one of the widely used models in which the mass rates in evaporation and condensation are modeled as:

$$\dot{m}^+ = C_e \frac{3\alpha_{nuc}\left(1-\alpha_v\right)\rho_v}{R_B}\left(\frac{2}{3}\frac{P_v - P}{\rho_l}\right)^{\frac{1}{2}} if\ P \le P_v \tag{10}$$

$$\dot{m}^- = C_c \frac{3\alpha_v \rho_v}{R_B}\left(\frac{2}{3}\frac{P - P_v}{\rho_l}\right)^{\frac{1}{2}} if\ P_v \le P \tag{11}$$

where α_{nuc} is the nucleation which is site volume fraction equaled to 5×10^{-4}. The other parameters are set as follows:

$$R_B = 10^{-6} \quad C_e = 50 \quad C_c = 0.001$$

4.4 Kunz Cavitation Model

Unlike the above-mentioned models, the Kunz (2000) cavitation model uses a different strategy. In this model, the mass source of the evaporation is a third-order polynomial function of volume fraction,γ, and the mass rate of condensation is directly proportional to the pressure difference, $P - P_v$ instead of the square root of it. The equations of mass source for this model are represented as follows:

$$\dot{m}^+ = \frac{C_e \rho_v \gamma (1-\gamma)}{t_\infty} \text{ if } P \le P_v \tag{12}$$

$$\dot{m}^- = \frac{C_c \rho_v \gamma \min[0, P - P_v]}{\left(\frac{1}{2}\rho_l {U_\infty}^2\right) t_\infty} \text{ if } P_v \le P. \tag{13}$$

The mean flow time scale is defined as $t_\infty = \frac{c}{U_\infty}$, where c is the chord length of hydrofoil and U_∞ is the free-stream velocity that is equal to the inlet velocity. The empirical coefficients, like to the original formulation, are set to:

$$C_e = 100 \quad C_c = 100$$

5 Turbulence Models

5.1 *SSTk − ω Model*

The shear–stress transport (SST) $k-\omega$ model was developed by Menter (1994) in 1994. This model has two transport equations, one for turbulent kinetic energy k and the other for energy dissipation rate ω**.**

$$\frac{\partial}{\partial t}(\rho k) + \frac{\partial}{\partial x_j}\left(\rho k u_j\right) = \tau_{ij}\frac{\partial u_i}{\partial x_j} + \frac{\partial}{\partial x_j}\left((\mu + \sigma_k \mu_t)\frac{\partial k}{\partial x_j}\right) - \beta^* \rho \omega k \tag{14}$$

$$\frac{\partial}{\partial t}(\rho \omega) + \frac{\partial}{\partial x_i}\left(\rho \omega u_i\right) = \frac{\gamma \omega}{k}\left(\tau_{ij}\frac{\partial u_i}{\partial x_j}\right) + \frac{\partial}{\partial x_j}\left(\left(\mu + \sigma_\omega \mu_t\right)\frac{\partial \omega}{\partial x_j}\right) + 2\left(1 - F_1\right)\frac{\rho \sigma_{\omega 2}}{\omega}\frac{\partial k}{\partial x_j}\frac{\partial \omega}{\partial x_j} - \beta \rho \omega^2. \tag{15}$$

If ϕ_1 denotes every constant in original $k-\omega$ model, ϕ_2 every constant in $k-\varepsilon$ model, and ϕ is indicative of every constant of *SST* $k-\omega$ model, there is a linear relation between them:

$$\phi = F_1 \phi_1 + \left(1 - F_1\right)\phi_2. \tag{16}$$

The variables of above equations are defined as follows**:**

$$\tau_{ij} = \mu_t\left(2\left(\frac{1}{2}\left(\frac{\partial u_i}{\partial x_j} + \frac{\partial u_j}{\partial x_i}\right)\right) - \frac{2}{3}\frac{\partial u_k}{\partial x_k}\delta_{ij}\right) - \frac{2}{3}\rho k \delta_{ij} \tag{17}$$

$$\mu_t = \frac{\rho \alpha_1 k}{max(\alpha_1 \omega, \Omega F_2)} \tag{18}$$

where Ω is an invariant measure of strain rate.

$$F_1 = \tanh\left(\min\left[\max\left(\frac{\sqrt{k}}{\beta^* \omega d}, \frac{500\vartheta}{d^2 \omega}\right), \frac{4\rho\sigma_{\omega 2} k}{CD_{k\omega} d^2}\right]^4\right) \tag{19}$$

$$F_2 = \tanh\left(max\left(2\frac{\sqrt{k}}{\beta^* \omega d}, \frac{500\vartheta}{d^2 \omega}\right)^2\right) \tag{20}$$

Default constants of this model are as follows:

$$\beta^* = 0.09 \quad \alpha_1 = 0.31 \quad \sigma_{\omega 2} = 0.856$$

5.2 SST Transition Model

This four-equation model is proposed in 2009 by Menter and Langtry (2009). It is based on the coupling of $SSTk-\omega$ transport equations with two other equations, one for the intermittency and the other for the transition onset criteria in terms of momentum-thickness. The intermittency Υ can be determined using the following equation:

$$\frac{\partial(\rho \Upsilon)}{\partial t} + \frac{\partial(\rho U_j \Upsilon)}{\partial x_j} = P_\Upsilon - E_\Upsilon + \frac{\partial}{\partial x_j}[\left(\mu + \frac{\mu_t}{\sigma_\Upsilon}\right)\frac{\partial \Upsilon}{\partial x_j}. \tag{21}$$

The transition source is defined as follows:

$$P_\Upsilon = F_{\text{length}} c_{a1} \rho S\left[\Upsilon F_{\text{onset}}\right]^{0.5}(1 - c_{e1}\Upsilon) \tag{22}$$

where S is the strain-rate magnitude. F_{length} is an empirical correlation that controls the length of the transition region, and F_{onset} controls the transition onset location. The destruction/relaminarization source is expressed as:

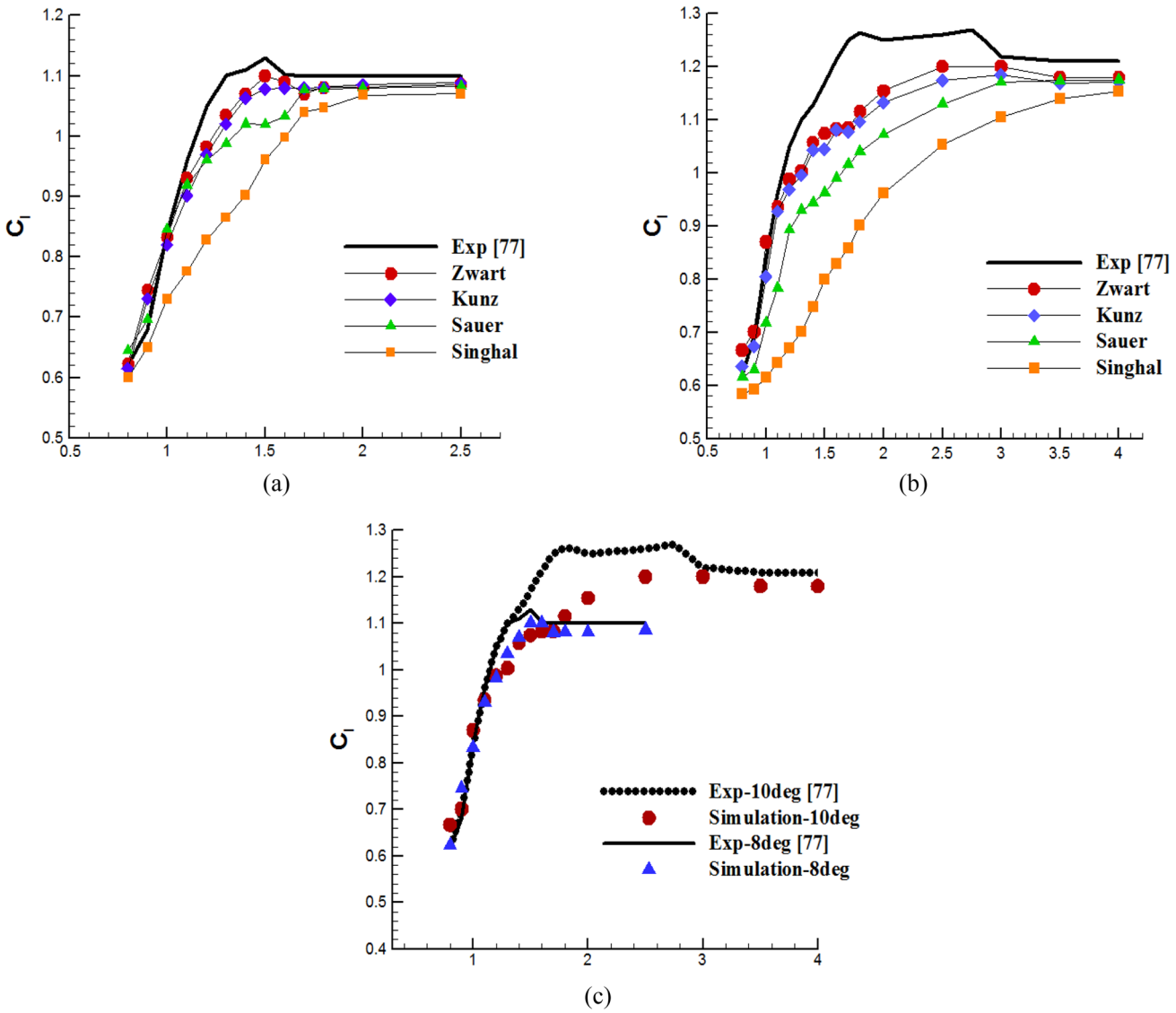

Fig. 6 Lift coefficient: **a** 8 deg, **b** 10 deg, and **c** comparison of 8 deg and 10 deg

$$E_{\Upsilon} = c_{a2}\rho\Omega\Upsilon F_{turb}(c_{e2}\Upsilon - 1) \tag{23}$$

where Ω is the magnitude of vorticity. The constants of intermittency equation are:

$$c_{e1} = 1 \quad c_{e2} = 50 \quad c_{a1} = 2 \quad c_{e2} = 0.06 \quad \sigma_{\gamma} = 1$$

The transport equation for the transition momentum-thickness Reynolds number $\widetilde{Re}_{\theta t}$ is determined using the following expression:

$$\frac{\partial(\rho\widetilde{Re}_{\theta t})}{\partial t} + \frac{\partial(\rho U_j\widetilde{Re}_{\theta t})}{\partial x_j} = P_{\theta t} + \frac{\partial}{\partial x_j}\left[\sigma_{\theta t}\left(\mu + \mu_t\right)\frac{\partial\widetilde{Re}_{\theta t}}{\partial x_j}\right]. \tag{24}$$

The source term of the above equation is:

$$P_{\theta t} = c_{\theta t}\frac{\rho}{t}(Re_{\theta t} - \widetilde{Re}_{\theta t})(1 - F_{\theta t}) \tag{25}$$

$$t = \frac{500\mu}{\rho U^2} \tag{26}$$

where t is the time scale and $F_{\theta t}$ is the blending function. $F_{\theta t}$ is equal to 0 in the free-stream flow and 1 inside of the boundary layer. The blending function $F_{\theta t}$ is not active in the wake regions downstream of an airfoil. The constants of the $\widetilde{Re}_{\theta t}$ transport equation are set to as follows:

$$c_{\theta t} = 0.03 \ \sigma_{\theta t} = 2$$

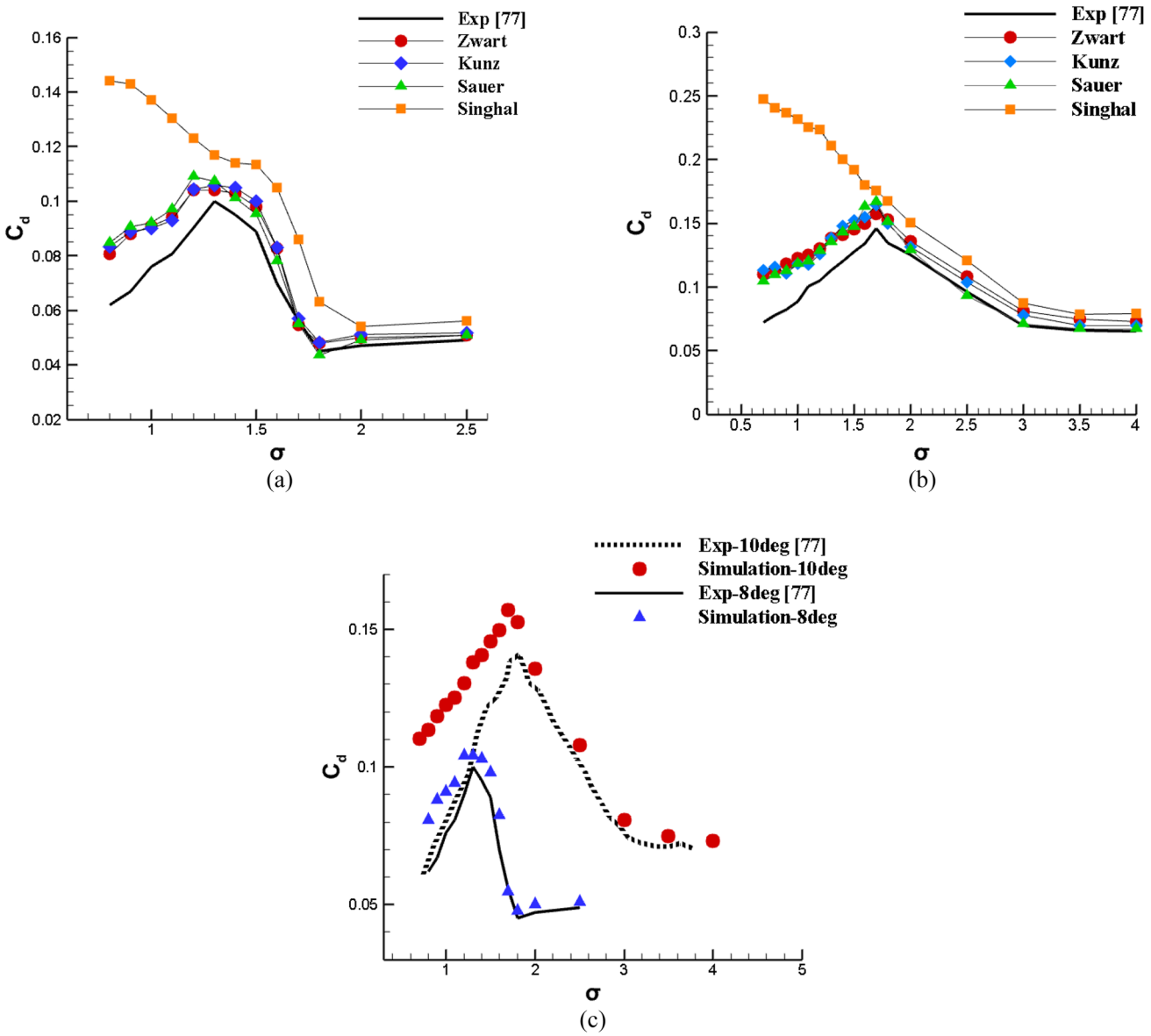

Fig. 7 Drag coefficient: **a** 8 deg, **b** 10 deg, and **c** comparison of 8 and 10 deg

6 $k-kl-\omega$ Model

In 2008, Walter et al. (2008) presented a turbulence model to predict boundary layer development and calculate transition onset. This model has three transport equations:

One for turbulent kinetic energy k_T, one for laminar kinetic energy k_L, and one for the inverse turbulent time scale ω:

$$\frac{Dk_T}{Dt} = P_{K_T} + R_{\mathrm{BP}} + R_{\mathrm{NAT}} - \omega_{K_T} - D_T + \frac{\partial}{\partial x_j}\left[\left(\nu + \frac{\alpha_T}{\sigma_K}\right)\frac{\partial k_T}{\partial x_j}\right] \tag{27}$$

$$\frac{Dk_L}{Dt} = P_{K_L} - R_{\mathrm{BP}} - R_{\mathrm{NAT}} - D_L + \frac{\partial}{\partial x_j}\left[\nu\frac{\partial k_L}{\partial x_j}\right] \tag{28}$$

$$\begin{aligned}\frac{D\omega}{Dt} =& C_{\omega 1}\frac{\omega}{K_T}P_{K_T} + \left(\frac{C_{\omega R}}{f_W} - 1\right)\frac{\omega}{K_T}\left(R + R_{\mathrm{NAT}}\right) \\ &- C_{\omega 2}\omega^2 + C_{\omega 3}\left(1 - \exp\left[-0.41\left(\frac{\lambda_{\mathrm{eff}}}{\lambda_T}\right)^4\right]\right)\alpha_T {f_W}^2\frac{\sqrt{K_T}}{d^3} \\ &+ \frac{\partial}{\partial x_j}\left[\left(\nu + \frac{\alpha_T}{\sigma_\omega}\right)\frac{\partial \omega}{\partial x_j}\right]\end{aligned} \tag{29}$$

$$K_{\mathrm{TOT}} = K_L + K_T. \tag{30}$$

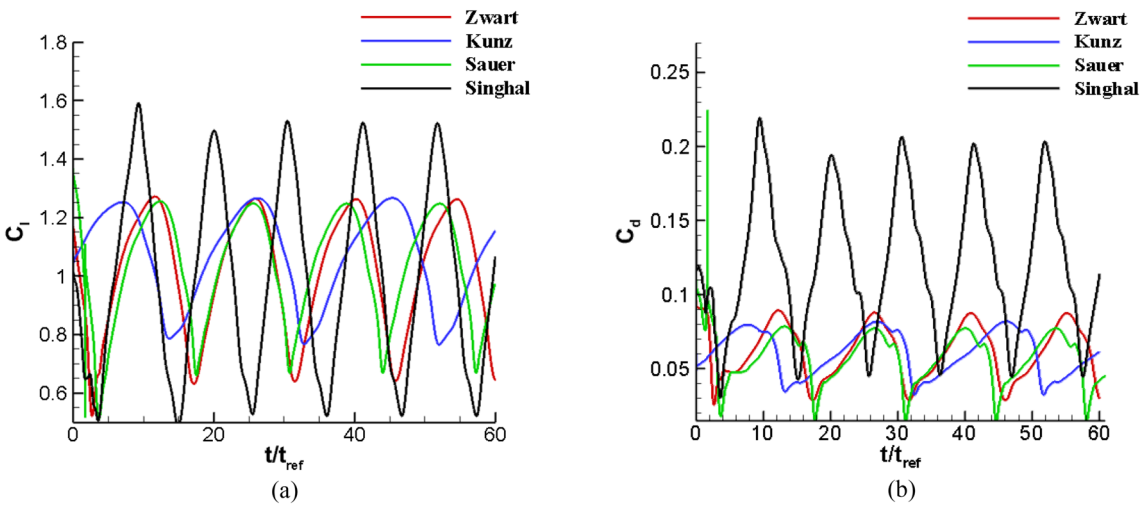

Fig. 8 Time variant hydrodynamic coefficients at $\sigma = 1.6$ and AOA = 8 deg: **a** C_l and **b** C_d

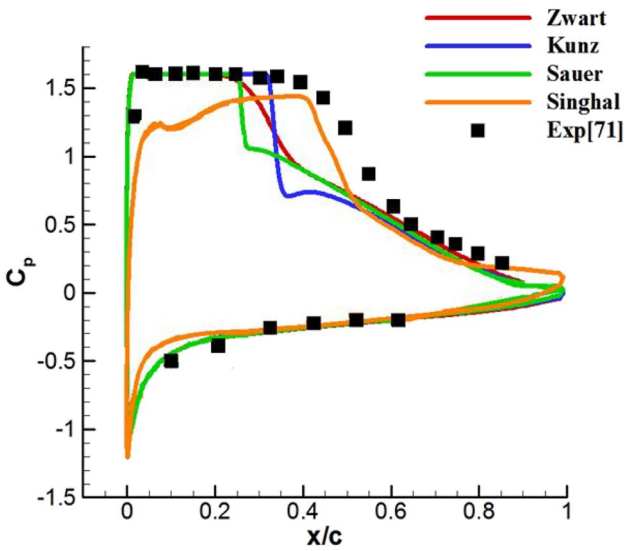

Fig. 9 Wall pressure coefficients on hydrofoil surface for $\sigma = 1.6$ and AOA = 8 deg

P_{K_T} and P_{K_L} are the production terms of turbulent and laminar kinetic energy, respectively, and modeled using strain rate. The model terms R_{BP} and R_{NAT} demonstrate bypass and natural transition, respectively.

$$R_{\mathrm{BP}} = C_R \beta_{\mathrm{BP}} K_L \omega / f_W \tag{31}$$

$$R_{\mathrm{NAT}} = C_{R,\mathrm{NAT}} \beta_{\mathrm{NAT}} K_L \Omega \tag{32}$$

β_{BP} and β_{NAT} are the threshold functions that the transition initiation is achievable employing them.

The model constants are:

$$C_{\omega 1} = 0.44 \quad C_{\omega 2} = 0.92 \quad C_{\omega 3} = 0.3$$
$$C_{\omega R} = 1.5 \quad \sigma_K = 1 \quad \sigma_\omega = 1.17$$

7 Results

7.1 Comparison of Cavitation Models

To compare and evaluate the performance of cavitation models from a hydrodynamic point of view, time-averaged lift and drag coefficients for different cavitation numbers; From non-cavitating flow to cloud cavitation regime is investigated. According to Wang et al. (2001) and Watanabe et al. (2014), Fig. 6 shows that in the non-cavitating flow, for cavitation numbers of 2.5–1.6, the lift coefficient C_l is almost constant. When incipient cavitation occurs, traveling bubbles can be observed in the flow and the lift coefficient increases slightly due to traveling cavities ($\sigma = 1.6 - 1.45$). Further decreasing the cavitation number, stable sheet cavitation occurs. The lift coefficient gradually decreases and takes the local minimum, and then just a small increase in C_l happens again. Afterward, the cavity becomes unstable and its length starts to oscillate with the detachment of cloud cavities from the trailing edge. At this stage, cavity shedding and related unsteady movements strongly affect the flow structure around the hydrofoil and the lift coefficient decreases. Finally, from the cloud cavitation stage, the cavity strongly fluctuates and C_l steeply becomes lower. Four cavitation models, Zwart, Kunz, Sauer, and Singhal models, have been applied and are compared in Fig. 6. Part (a) of this figure denotes that in the range of inception to the unstable partial cavitation, simulations do have not enough accuracy

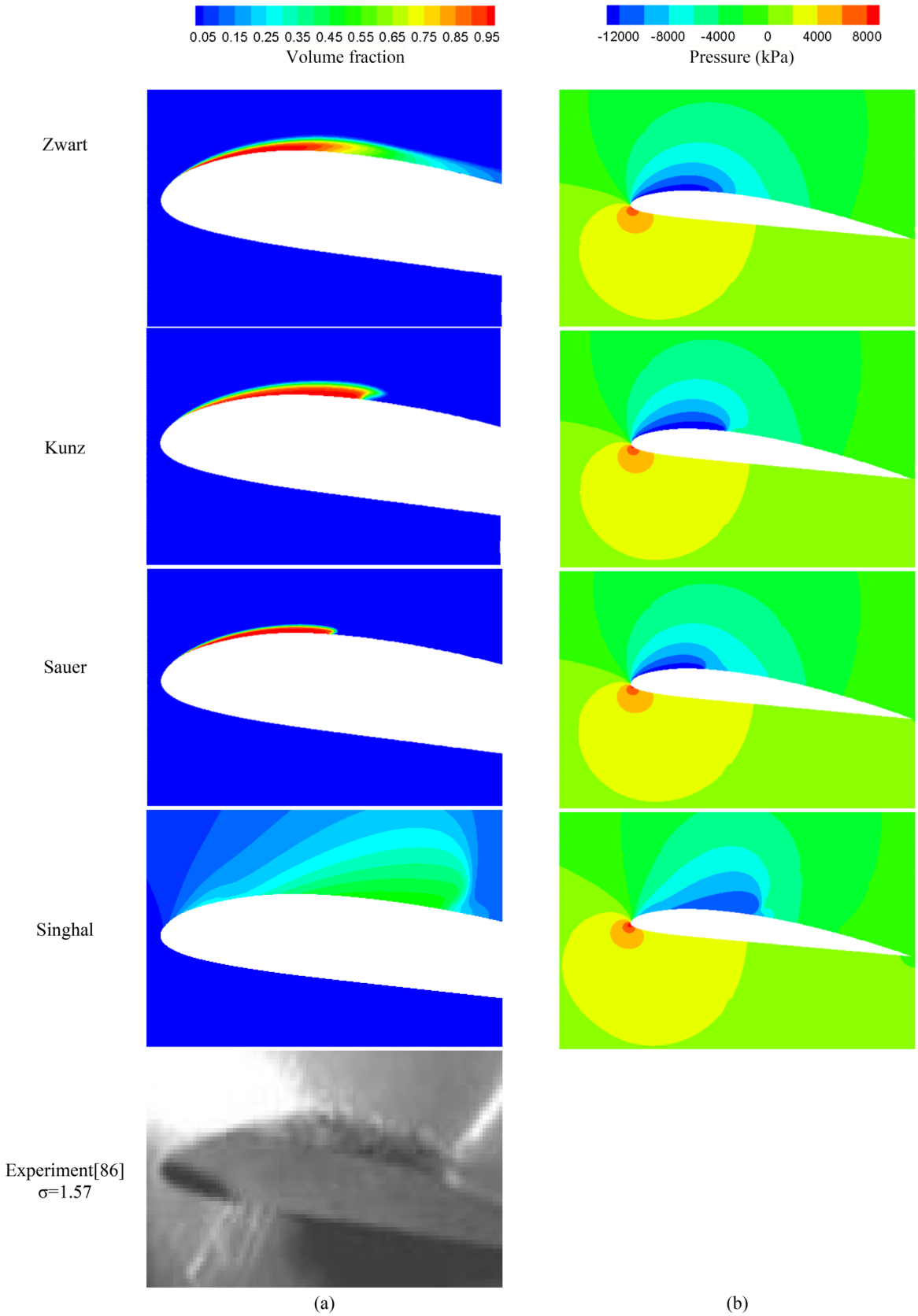

Fig. 10 Cavitation characteristics of different mass transfer models at σ = 1.6 and AOA = 8 deg compared to experiments (Tsuru 2018): **a** vapor volume fraction and **b** pressure distribution

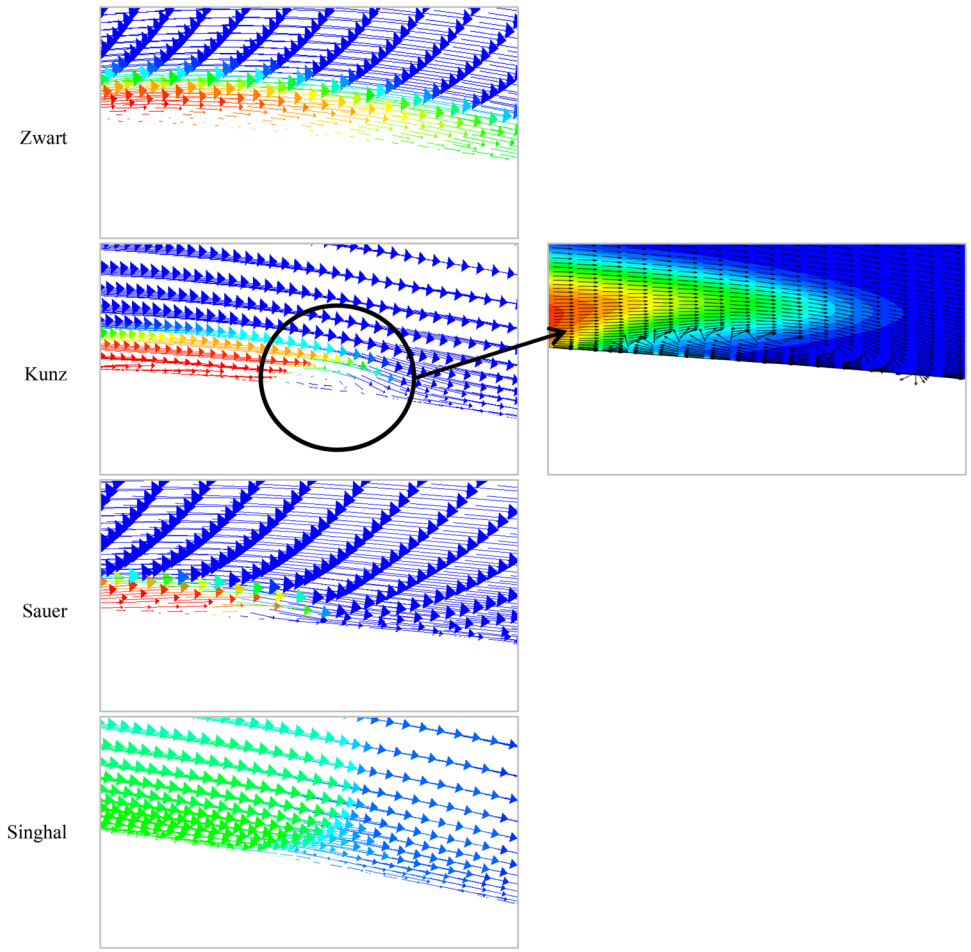

Fig. 11 Velocity vectors colored by vapor volume fraction at $\sigma = 1.6$

for the prediction of the lift coefficient. Singhal and Sauer models exhibit a uniform reduction of C_l, while Zwart and Kunz models have the same trend as the experimental data. However, lift increment due to inception is more sensible in the Zwart model. We can see from Fig. 6 that CFD modeling predicts the inception of cavitation in a larger cavitation number than experiments. It is because the cavity is very small when cavitation starts and it is difficult to see it with the naked eye in the experiment, whereas it is clearly visible in the simulations. For more assurance, a similar work was repeated for AOA = 10 deg. Part (b) of this figure shows that the obtained results confirm the information provided in part (a). With the aim of better understanding of lift variation mechanism and mass transfer models proficiency in different angles of attack, we compared C_l from Zwart model with the measured data for 8 deg and 10 deg angles of attack. Figure 6. (c) indicates that C_l has higher values as the angle of attack becomes larger. In addition, the inception to sheet/cloud region is bigger in 10 deg and the difference between experiments and simulations is more notable.

Like the lift coefficient, the drag coefficient also remains nearly unchanged in the non-cavitating flow. From incipient cavitation to unstable sheet cavitation, C_d increases monotonously and reaches the maximum value, then decreases with the development of cavitation. Figure 7 represents drag coefficients in different cavitation numbers for 8 and 10 degree angles of attack, respectively. Singhal model predicts a unison increase in drag coefficient from non-cavitating to cloud cavitation regime, but the other models' trend is similar to the measured data. All the mass transfer models over-predict C_d, and the results of Zwart, Sauer, and Kunz models are very close together. It should be pointed out that before the cloud cavitation, CFD results are in good agreement with experiments but with the onset of the cloud regime, more differences can be seen. From Fig. 7.c, we realize that the larger angle of attack, the higher value of C_d. In the case of drag coefficient, for bigger angles, the cavitation models have less precision in the cloud region.

Figure 8 demonstrates time variations of lift and drag coefficients for several periods at $\sigma = 1.6$ and AOA = 8 deg. The fluctuation of C_l and C_d against time is representative

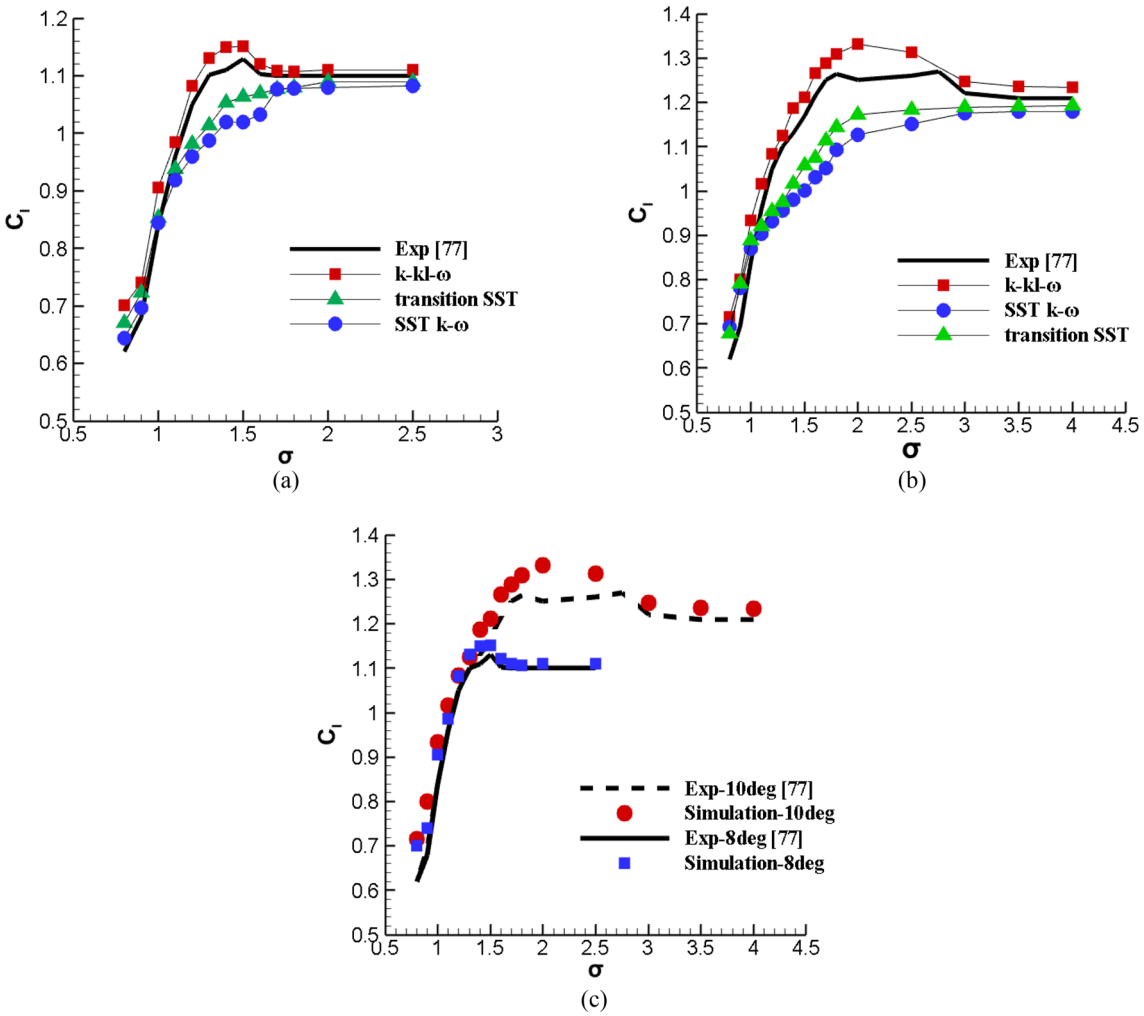

Fig. 12 Lift coefficients: **a** 8 deg, **b** 10 deg, and **c** comparison of 8 deg and 10 deg

of the inherent unsteady nature of partial cavitation. As can be observed, Singhal model has the largest amplitude and the smallest periods. On the contrary, the minimum amplitude and the maximum period belong to Kunz model. This means Singhal model has the maximum frequency and less stability among the other mass transfer models. On the other hand, Kunz model has the minimum frequency and the most stability compared to other models.

Figure 9 shows cavitation models pressure coefficients on the suction side of hydrofoil at the inception stage,$\sigma = 1.6$ and AOA = 8 deg**.** According to Brennen (2014) and Passandideh-Fard et al. (2008), the pressure coefficient inside of cavity conforms to the cavitation number ($\sigma = -C_{p_{\min}}$). It can be found from Fig. 9 that Singhal model doesn't meet this condition and its C_p increases at (0.1–0.45)c. Furthermore, there is an adverse pressure gradient after the cavity closure region. Plainly from Figs. 9 and 10, the cavity region predicted by Kunz model is longer, its shape and closure region is completely clear. After cavity closure,C_p drastically reduces which means this model appraises a big pressure gradient. Sauer model evaluates both cavity length and pressure gradient fewer than Kunz model. Besides, in Zwart model, cavity closure is longer and C_p smoothly decreases. It is inferred that Zwart model considers a smaller pressure gradient than the rest of the cavitation models. Figure 11 shows the velocity vectors colored by vapor volume fraction around the hydrofoil surface. Obviously, none of the mass transfer

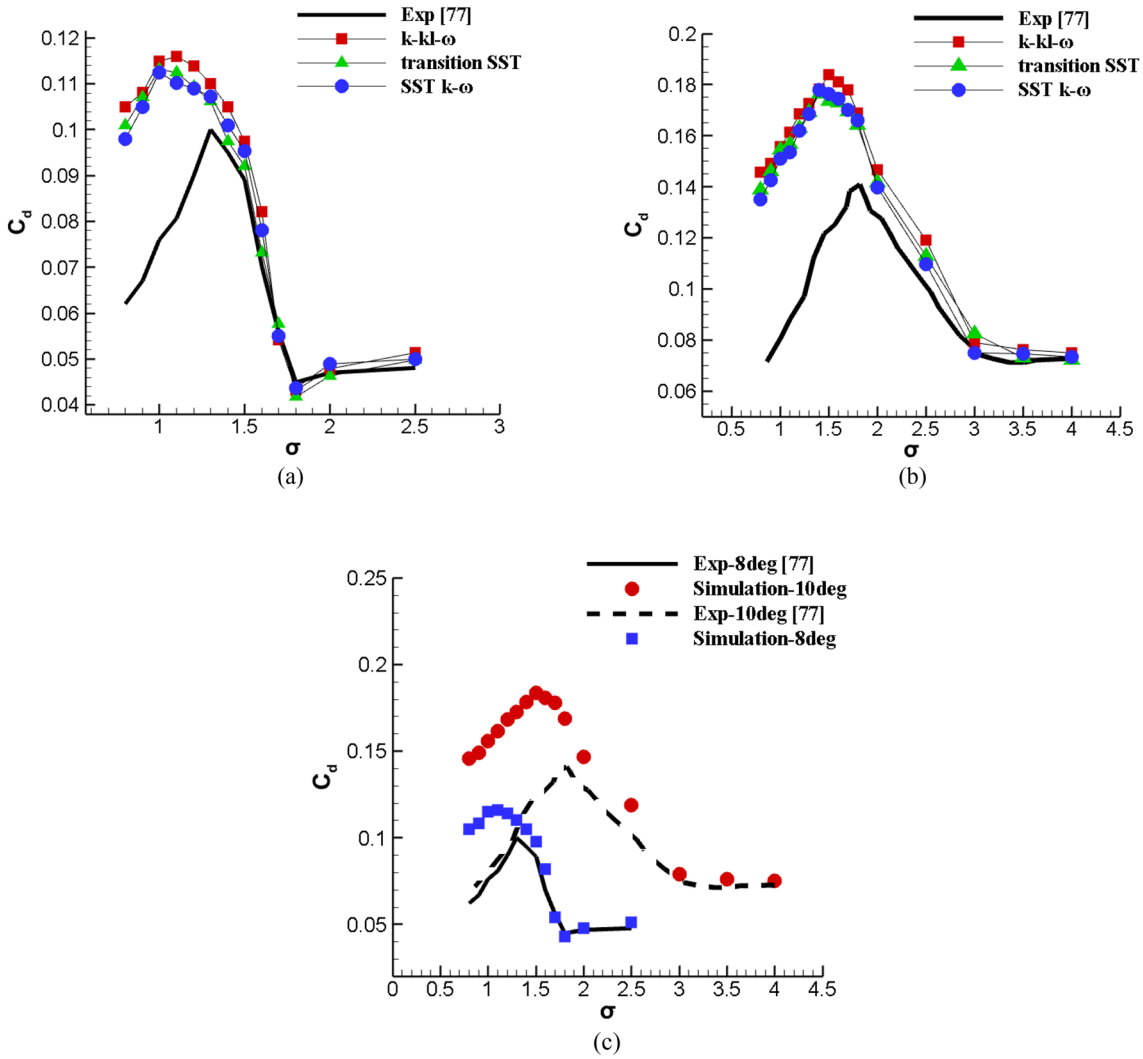

Fig. 13 Drag coefficients: **a** 8 deg, **b** 10 deg, and **c** comparison of 8 and 10 deg

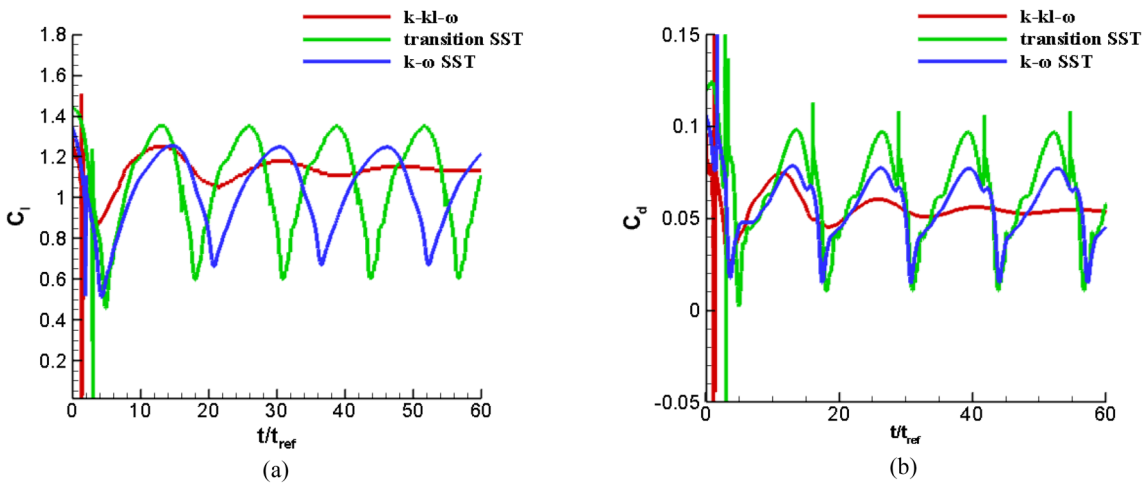

Fig. 14 Time variant hydrodynamic coefficients at $\sigma = 1.6$ and AOA = 8 deg: **a** C_l and **b** C_d

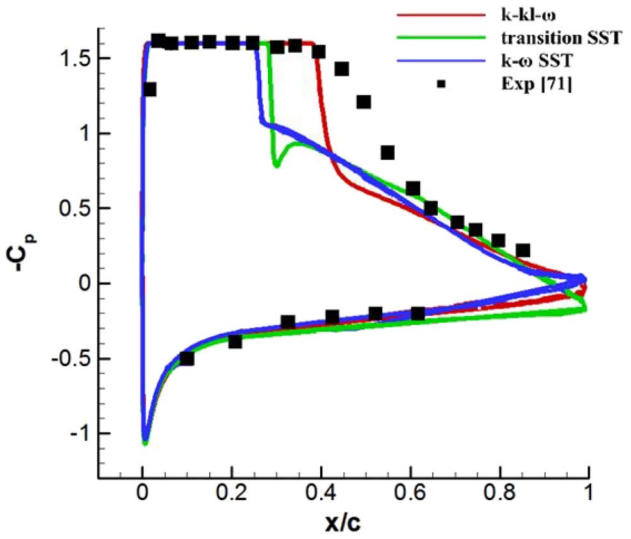

Fig. 15 Wall pressure coefficient on the hydrofoil surface, $\sigma = 1.6$ and AOA = 8 deg

models except Kunz model can predict re-entrant jet at the cavity tail, which strongly affects the flow unsteadiness and causes instabilities leading to the cavity length oscillations.

7.2 Comparison of Turbulence Models

Figure 12a and b compares the capability of different turbulence models in computing C_l against the experimental data for the 8 and 10 degree angles, respectively. The results show that the $k-kl-\omega$ model over-predicts and the other models under-predict the lift coefficient. SST$k-\omega$ and SSTtransition models have a descending tendency but $k-kl-\omega$ has an ascending–descending trend same as measured data. Turbulence models mainly differ in the unstable sheet cavitation stage and the $k-kl-\omega$ model has more accordance with the experiments. From Fig. 12c, it is clearly deduced that as the angle of attack increases, the precision of the models in lift estimation reduces. Turbulence models sufficiency in the prediction of drag coefficients for 8 and 10 degree angels is displayed in Fig. 13 a and b, respectively. The C_d values of all three models are closed together and have similar trends as experiments. Before the cloud cavitation regime, the results are well agreed with experimental data, but after then, significant differences can be seen. Figure 13c depicts that turbulent models act more precisely in the case of small angles of attack. Similar to what was mentioned earlier in Sect. 6.1, Fig. 14 represents that the $k-kl-\omega$ model has the minimum frequency, more stability, and better convergence with respect to the other turbulence models. Figures 15 and 16 exhibit that the $k-kl-\omega$ model calculates cavity length and adverse pressure gradient more than the other two turbulence models. There is no significant difference between predicted cavity length by SST $k-\omega$ and SST*transition* models, but the SST*transition* model computes a sharper pressure gradient.

7.3 Unsteady Results at AOA = 8 deg and Cavitation Number of 1.45

As Figs. 6(a) and 12(a) show, the maximum lift coefficient occurs at 1.45 cavitation number which slightly increases after initial cavitation. Figure 17 illustrates the vapor volume fraction, pressure coefficient, and cavity length on the hydrofoil surface at different fractions of time in an oscillating period T. As can be seen, the cavity grows until 5 T/8 with the maximum length. After this time, the cavity shrinks and the end of the cavity fills with water due to the re-entrant jet working. The minimum length of the cavity takes place at the end of the time period with the 0.353th of chord length and minimum values of lift and drag coefficients.

To investigate the pressure variation on the upper surface of the hydrofoil against the time, 11 points have been specified with equal distances. Figure 18 shows the pressure coefficient variations at each point for different stages of time in an oscillating time period. First, it must be mentioned that the cavity starts slightly after $x/c = 0$. Secondly, those points located between $x/c = 0.1$ to $x/c = 0.3$ are always in the cavity without somewhat pressure variation. Further, for the points with $x/c = 0.4$ and 0.5, we see the cavity with the minimum pressure for sometimes, although this time duration for $x/c = 0.5$ is less. For the points at $x/c = 0.6$ and 0.7, we have no cavitation, but because of being close to the cavity condition, the pressure is influenced. Finally, for the region after $x/c = 0.8$ until the trailing edge the pressure is approximately constant and does not vary with time considerably.

8 Conclusions

Cavitating flows occur in a wide range of practical cases and can be modeled through various methods. In the present study, we used four cavitation and three turbulence models to simulate cavitating flow from non-cavitating to cloud conditions over a 2D ClarkY11.7% at 8° and 10° angles of attack. For this purpose, the time-averaged lift and drag coefficients obtained from different models, are compared to the experimental data. In the case of lift coefficients, all of the models predict lower values respect to the experiments. Zwart model has the same trend to the experiments and closer values to measured data. On the other hand, $k-kl-\omega$ turbulence model has over-prediction and the same trend as experiments. In the case of drag coefficient, cavitation models over-predict the values, Singhal model

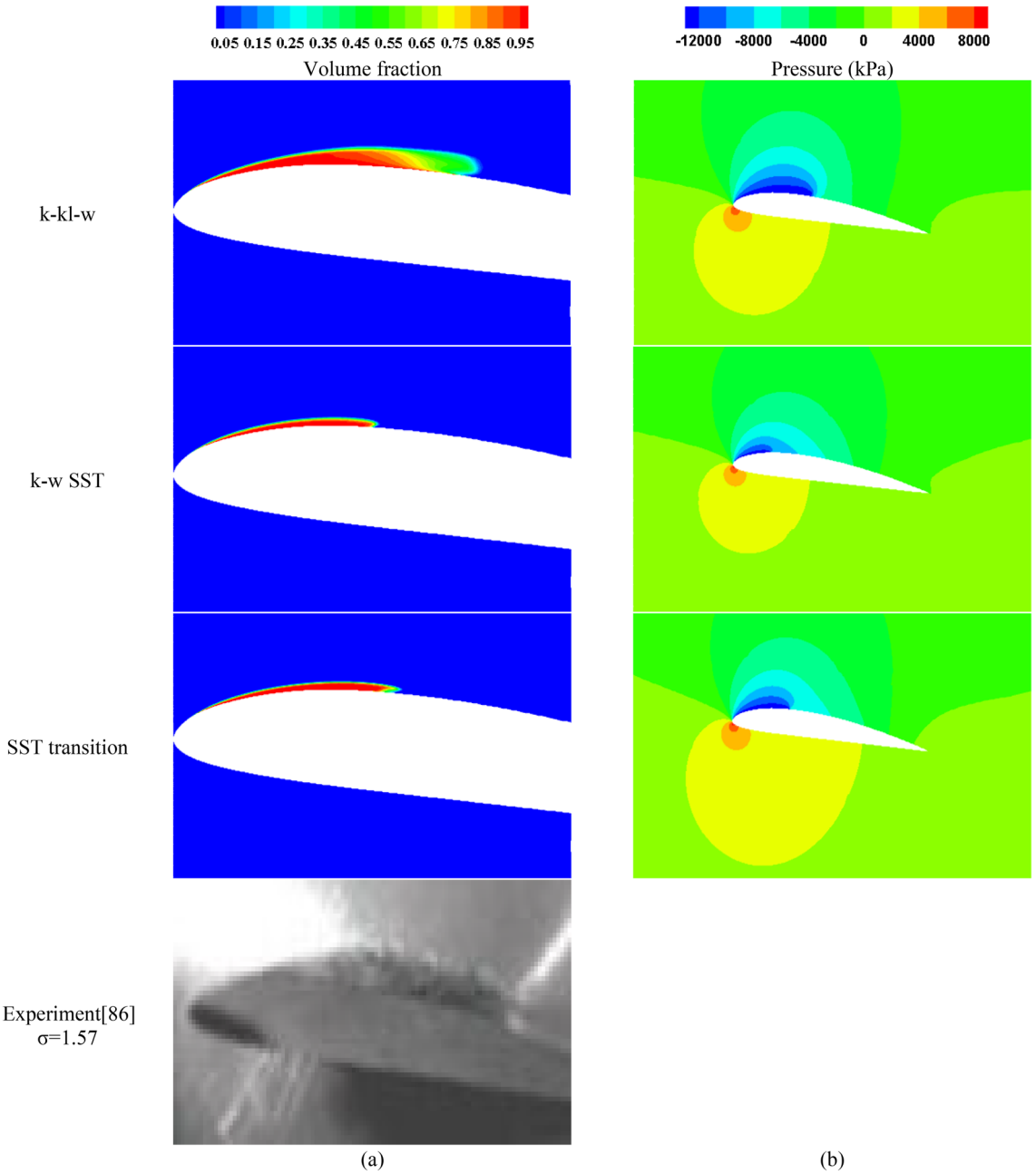

Fig. 16 Cavitation characteristics of different turbulence models at $\sigma = 1.6$ and AOA = 8 deg compared to experiments (Tsuru 2018): **a** vapor volume fraction and **b** pressure distribution

shows a uniform increase in this coefficient, but the other models have close values to each other and same the trend as experiments. As well as, the turbulence models don't differ much in C_d values. Time variant coefficients of lift and drag, in the cavitation inception point ($\sigma = 1.6$), confirm the oscillatory behavior of the cavity. Unlike the other cavitation models, the Kunz model shows the re-entrant jet in the cavity tail which is the reason for cavity oscillations and causes more unsteadiness in the flow structure. Also, the cavity length predicted by Kunz and $k - kl - \omega$ models is in more agreement with the measured data, however, Zwart model presents a better prediction of the vapor region at the end of the cavity tail. Consequently, using Kunz or Zwart cavitation models in unison with $k - kl - \omega$ turbulence model can provide more accurate results in the simulation of the incipient to unsteady sheet/cloud cavitation flows.

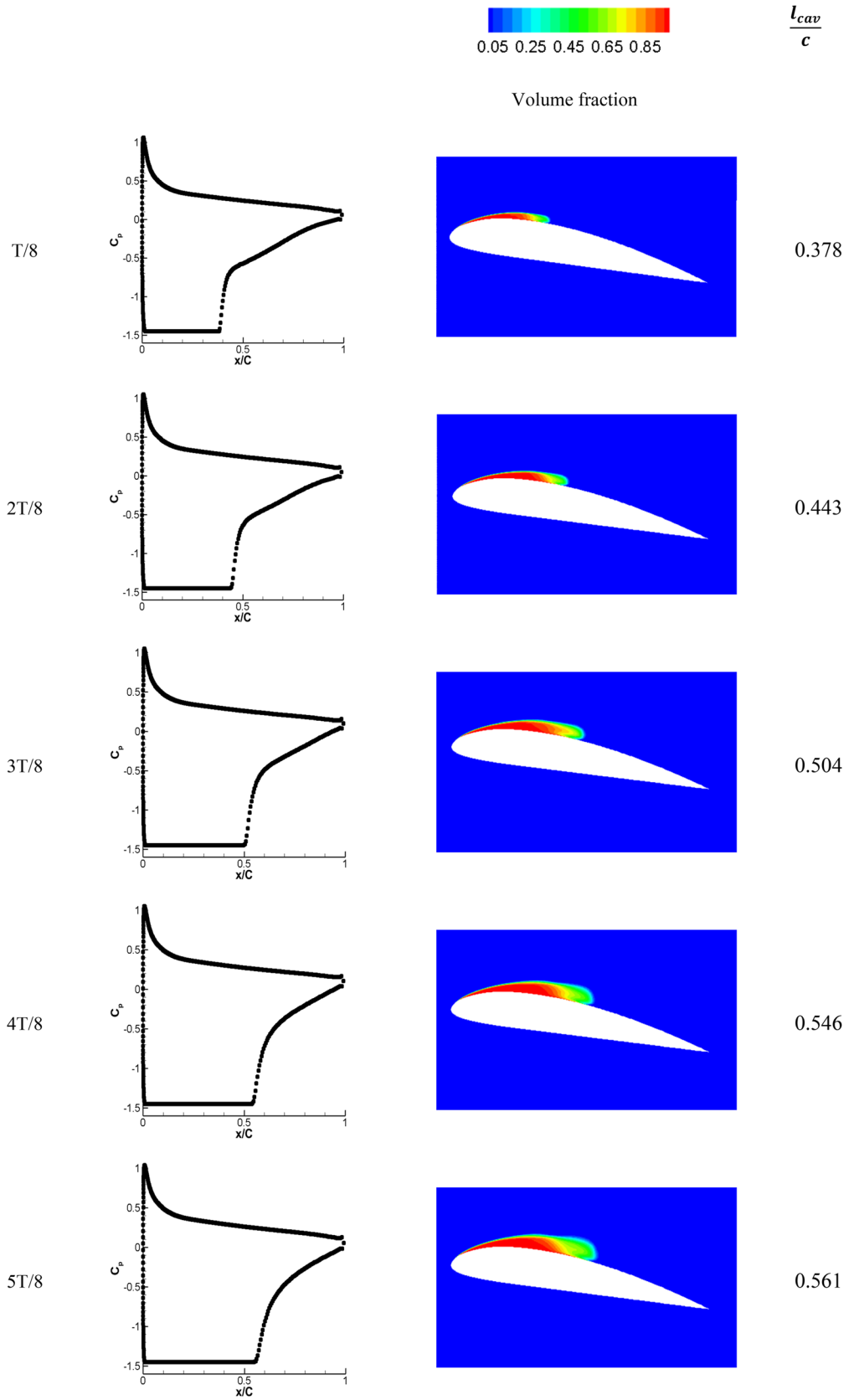

Fig. 17 **a** Pressure coefficients and **b** vapor volume fraction contours in an oscillating period of time T at σ=1.45 on the hydrofoil surface

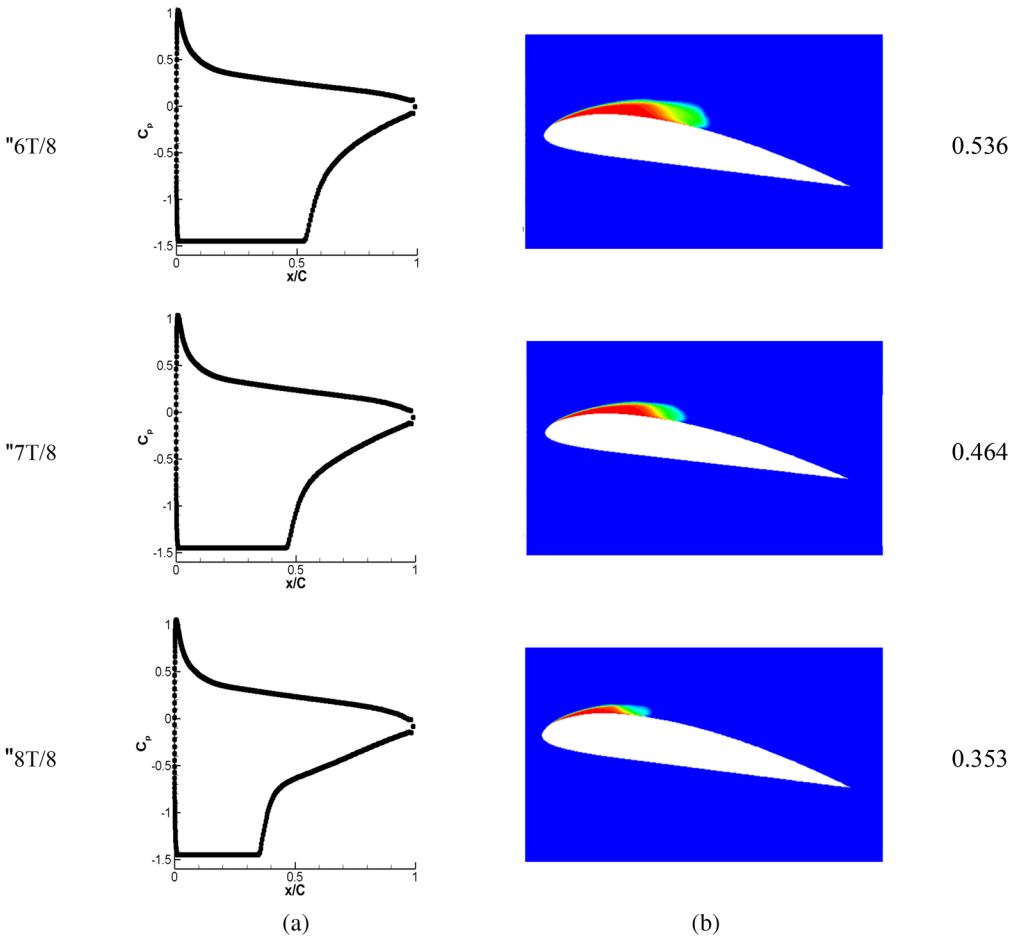

Fig. 17 (continued)

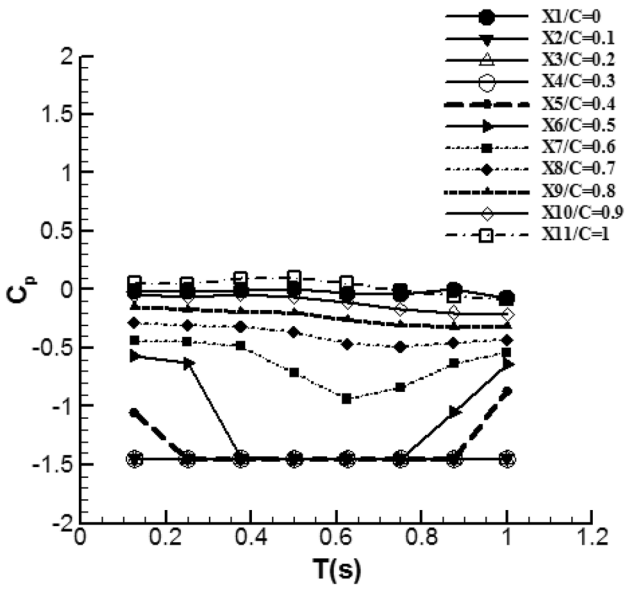

Fig. 18 Variations of pressure coefficient with time for 11 points with equal distances on the top surface of ClakY11.7% hydrofoil in an oscillating time period at 8 deg angle of attack and σ=1.45

References

Bensow RE, Bark G (2010) "Simulating cavitating flows with LES in OpenFoam," In: V European conference on computational fluid dynamics, pp 14–17

Brennen CE (2014) Cavitation and bubble dynamics. Cambridge University Press, Cambridge

Capurso T et al (2017) Numerical investigation of cavitation on a NACA0015 hydrofoil by means of OpenFOAM. Energy Procedia 126:794–801

Causon DM, Mingham CG (2013) Finite volume simulation of unsteady shock-cavitation in compressible water. Int J Numer Methods Fluids 72(6):632–649

Cheng X, Jia N, Lv B, Chen H (2020) Effect of meridian plane dip angle of the variable pitch inducer blade on cavitation performance of high-speed centrifugal pump. J Braz Soc Mech Sci Eng 42(5):217. https://doi.org/10.1007/s40430-020-02289-3

Corson D, Jaiman R, Shakib F (2009) Industrial application of RANS modelling: capabilities and needs. Int J Comut Fluid Dyn 23(4):337–347

Coussirat MG, Moll FH, Fontanals A (2016a) Capability of the present cavitating and turbulence models for confined flow simulations. Mecánica Comput 34(29):1989–2007

Coussirat M, Moll F, Cappa F, Fontanals A (2016b) "Study of available turbulence and cavitation models to reproduce flow patterns in confined flows," J Fluids Eng, 138(9)
Coutier-Delgosha O, Reboud J-L, Fortes-Patella R (2002) Numerical study of the effect of the leading edge shape on cavitation around inducer blade sections. JSME Int J Ser B Fluids Therm Eng 45(3):678–685
Coutier-Delgosha O, Reboud JL, Delannoy Y (2003a) Numerical simulation of the unsteady behaviour of cavitating flows. Int J Numer Methods Fluids 42(5):527–548
Coutier-Delgosha O, Fortes-Patella R, Reboud J-L (2003b) Evaluation of the turbulence model influence on the numerical simulations of unsteady cavitation. J Fluids Eng 125(1):38–45
Coutier-Delgosha O, Fortes-Patella R, Reboud J-L, Hakimi N, Hirsch C (2005) Stability of preconditioned Navier-Stokes equations associated with a cavitation model. Comput Fluids 34(3):319–349
Coutier-Delgosha O, Deniset F, Astolfi JA, Leroux J-B (2007) Numerical prediction of cavitating flow on a two-dimensional symmetrical hydrofoil and comparison to experiments
Decaix J, Goncalves E (2012) Time-dependent simulation of cavitating flow with k– ℓ turbulence models. Int J Numer Methods Fluids 68(8):1053–1072
Delannoy Y (1990) Two phase flow approach in unsteady cavitation modelling
Ducoin A, Huang B, Young YL (2012) Numerical modeling of unsteady cavitating flows around a stationary hydrofoil. Int J Rotating Mach 2012:1–17
Dular M, Coutier-Delgosha O (2009) Numerical modelling of cavitation erosion. Int J Numer Methods Fluids 61(12):1388–1410
Erfanian MR, Anbarsooz M (2018) Numerical investigation of body and hole effects on the cavitating flow behind a disk cavitator at extremely low cavitation numbers. Appl Math Model 62:163–180
Frikha S, Coutier-Delgosha O, Astolfi JA (2008) Influence of the cavitation model on the simulation of cloud cavitation on 2D foil section. Int J Rotating Mach 2008:1–12
Geng L, Escaler X (2020) Assessment of RANS turbulence models and Zwart cavitation model empirical coefficients for the simulation of unsteady cloud cavitation. Eng Appl Comput Fluid Mech 14(1):151–167
Goncalvès E (2011) Numerical study of unsteady turbulent cavitating flows. Eur J Mech 30(1):26–40
Goncalvès E (2013) Numerical study of expansion tube problems: toward the simulation of cavitation. Comput Fluids 72:1–19
Goncalvès E, Patella RF (2011) Constraints on equation of state for cavitating flows with thermodynamic effects. Appl Math Comput 217(11):5095–5102
Goncalves E, Patella RF (2009) Numerical simulation of cavitating flows with homogeneous models. Comput Fluids 38(9):1682–1696
Gopalan S, Katz J (2000) Flow structure and modeling issues in the closure region of attached cavitation. Phys Fluids 12(4):895–911
Gosman AD (1999) Developments in CFD for industrial and environmental applications in wind engineering. J Wind Eng Ind Aerodyn 81(1–3):21–39
Hejranfar K, Hajihassanpour M (2017) A high-order nodal discontinuous Galerkin method for solution of compressible non-cavitating and cavitating flows. Comput Fluids 156:175–199
Hejranfar K, Ezzatneshan E, Fattah-Hesari K (2015) A comparative study of two cavitation modeling strategies for simulation of inviscid cavitating flows. Ocean Eng 108:257–275
Hong F, Yuan J, Zhou B (2017) Application of a new cavitation model for computations of unsteady turbulent cavitating flows around a hydrofoil. J Mech Sci Technol 31(1):249–260
Huang S, He M, Wang C, Chang X (2010) Simulation of cavitating flow around a 2-D hydrofoil. J Mar Sci Appl 9(1):63–68
Hutli E, Nedeljkovic M, Bonyár A (2019) Dynamic behaviour of cavitation clouds: visualization and statistical analysis. J Brazilian Soc Mech Sci Eng 41(7):1–15
Iga Y, Nohmi M, Goto A, Shin BR, Ikohagi T (2003) Numerical study of sheet cavitation breakoff phenomenon on a cascade hydrofoil. J Fluids Eng 125(4):643–651
Kolahan A, Roohi E, Pendar M-R (2019) Wavelet analysis and frequency spectrum of cloud cavitation around a sphere. Ocean Eng 182:235–247
Koop AH, Hoeijmakers H (2008) Numerical simulatin of unsteady three-dimensional sheet cavitation. University of Twente Enschede, The Netherlands
Kubota A, Kato H, Yamaguchi H (1992) A new modelling of cavitating flows: a numerical study of unsteady cavitation on a hydrofoil section. J Fluid Mech 240:59–96
Kunz RF et al (2000) A preconditioned Navier-Stokes method for two-phase flows with application to cavitation prediction. Comput Fluids 29(8):849–875
Langtry RB, Menter FR (2009) Correlation-based transition modeling for unstructured parallelized computational fluid dynamics codes. AIAA J 47(12):2894–2906
LarKermani E, Roohi E, Porté-Agel F (2018) Evaluating the modulated gradient model in large eddy simulation of channel flow with OpenFOAM. J Turbul 19(7):600–620
Liu H, Wang Y, Liu D, Yuan S, Wang J (2013) Assessment of a turbulence model for numerical predictions of sheet-cavitating flows in centrifugal pumps? J Mech Sci Technol 27(9):2743–2750
Liu H, Wang J, Wang Y, Huang H, Jiang L (2014) Partially-averaged Navier-Stokes model for predicting cavitating flow in centrifugal pump. Eng Appl Comput Fluid Mech 8(2):319–329
Liuzzi D (2012) Two-Phase Cavitation Modelling
Lu NX, Svennberg U, Bark G, Bensow R (2012) Numerical simulations of the cavitating flow on a marine propeller
Matsunari H, Watanabe S, Konishi Y, Suefuji N, Furukawa A (2012) "Experimental/numerical study on cavitating flow around Clark Y 11.7% hydrofoil," In: Proceedings of eighth international symposium on cavitation, pp 358–363
Menter FR (1994) Two-equation eddy-viscosity turbulence models for engineering applications. AIAA J 32(8):1598–1605
Merkle CL (1998) Computational modelling of the dynamics of sheet cavitation
Morgut M, Nobile E, Biluš I (2011) Comparison of mass transfer models for the numerical prediction of sheet cavitation around a hydrofoil. Int J Multiph Flow 37(6):620–626
Movahedian A, Pasandidehfard M, Roohi E (2019) LES investigation of sheet-cloud cavitation around a 3-D twisted wing with a NACA 16012 hydrofoil. Ocean Eng 192:106547
Niu Y-Y, Lin Y-M, Lin Y-C (2007) A simple and robust advection upwind flux splitting to simulate transient cavitated water-vapor flows. Numer Heat Transf Part A Appl 51(7):679–696
Palau Salvador G, Frankel S (2004) "Numerical modeling of cavitation using fluent: validation and parametric studies," In: 34th AIAA fluid dynamics conference and exhibit, p 2642
Park S, Rhee SH (2012) Computational analysis of turbulent supercavitating flow around a two-dimensional wedge-shaped cavitator geometry. Comput Fluids 70:73–85
Passandideh-Fard M, Roohi E (2008) Transient simulations of cavitating flows using a modified volume-of-fluid (VOF) technique. Int J Comut Fluid Dyn 22(1–2):97–114
Pendar MR, Roohi E (2016) Investigation of cavitation around 3D hemispherical head-form body and conical cavitators using different turbulence and cavitation models. Ocean Eng 112:287–306
Pendar MR, Roohi E (2018) Cavitation characteristics around a sphere: an LES investigation. Int J Multiph Flow 98:1–23

Pendar MR, Esmaeilifar E, Roohi E (2020) LES study of unsteady cavitation characteristics of a 3-D hydrofoil with wavy leading edge. Int J Multiph Flow 132:103415

Qin Q, Song CCS, Arndt REA (2003) A virtual single-phase natural cavitation model and its application to Cav2003 hydrofoil

Reboud JL, Stutz B, Coutier O (1998) "Two phase flow structure of cavitation: experiment and modeling of unsteady effects," In: 3rd international symposium on cavitation CAV1998, Grenoble, France, vol. 26

Reboud JL, Coutier-Delgosha O, Pouffary B, Fortes-Patella R (2003) "Numerical simulation of unsteady cavitating flows: some applications and open problems," In: Fifth international symposium on cavitation, pp 1–10

Roohi E, Zahiri AP, Passandideh-Fard M (2013) Numerical simulation of cavitation around a two-dimensional hydrofoil using VOF method and LES turbulence model. Appl Math Model 37(9):6469–6488

Roohi E, Pendar M-R, Rahimi A (2016) Simulation of three-dimensional cavitation behind a disk using various turbulence and mass transfer models. Appl Math Model 40(1):542–564

Salim SM, Buccolieri R, Chan A, Di Sabatino S (2011) Numerical simulation of atmospheric pollutant dispersion in an urban street canyon: comparison between RANS and LES. J Wind Eng Ind Aerodyn 99(2–3):103–113

Saurel R, Cocchi JP, Butler PB (1999) Numerical study of cavitation in the wake of a hypervelocity underwater projectile. J Propuls Power 15(4):513–522

Schnerr GH, Sauer J (2001) "Physical and numerical modeling of unsteady cavitation dynamics," In: Fourth international conference on multiphase flow, vol. 1

Senocak I, Shyy W (2002) Evaluations of cavitation models for Navier-Stokes computations. Fluids Eng Div Summer Meet 36150:395–401

Senocak I, Shyy W (2004a) Interfacial dynamics-based modelling of turbulent cavitating flows, Part-1: model development and steady-state computations. Int J Numer Methods Fluids 44(9):975–995

Senocak I, Shyy W (2004b) Interfacial dynamics-based modelling of turbulent cavitating flows, Part-2: time-dependent computations. Int J Numer Methods Fluids 44(9):997–1016

Shin BR, Ikohagi T (1999) "Numerical analysis of unsteady cavity flows around a hydrofoil," ASME Pap. FEDSM, pp 99–7215

Singhal AK, Athavale MM, Li H, Jiang Y (2002) Mathematical basis and validation of the full cavitation model. J Fluids Eng 124(3):617–624

Song CCS (1998) Numerical simulation of cavitating flows by a single-phase flow approach

Štigler J, Svozil J (2009) Modeling of cavitation flow on NACA 0015 hydrofoil. Eng Mech 16(6):447–455

Tran TD, Nennemann B, Vu TC, Guibault F (2015) Investigation of cavitation models for steady and unsteady cavitating flow simulation. Int J Fluid Mach Syst 8(4):240–253

Tsuru W, Ehara S, Kitamura S, Watanabe S, Tsuda SI (2018) Mechanism of lift increase of cavitating Clark Y-11.7% hydrofoil

Ventikos Y, Tzabiras G (2000) A numerical method for the simulation of steady and unsteady cavitating flows. Comput Fluids 29(1):63–88

Walters DK, Cokljat D (2008) "A three-equation eddy-viscosity model for Reynolds-averaged Navier–Stokes simulations of transitional flow," J Fluids Eng, 130(12)

Wang G, Senocak I, Shyy W, Ikohagi T, Cao S (2001) Dynamics of attached turbulent cavitating flows. Prog Aerosp Sci 37(6):551–581

Wang S, Zhu J, Xie H, Zhang F, Zhang X (2019) Studies on thermal effects of cavitation in LN2 flow over a twisted hydrofoil based on large eddy simulation. Cryogen (Guildf) 97:40–49

Watanabe S, Yamaoka W, Furukawa A (2014) Unsteady lift and drag characteristics of cavitating Clark Y-11.7% hydrofoil. IOP Conf Series Earth Environ Sci 22(5):52009

Wienken W, Stiller J, Keller A (2006) A method to predict cavitation inception using large-eddy simulation and its application to the flow past a square cylinder

Wu P-C, Chen J-H (2016) Numerical study on cavitating flow due to a hydrofoil near a free surface. J Ocean Eng Sci 1(3):238–245

Yin T, Pavesi G, Pei J, Yuan S, Daniel NA (2018) Comparison of various turbulence models applied to a twisted hydrofoil. ASME, New York

Yu A, Tang Q, Zhou D (2019) Cavitation evolution around a NACA0015 hydrofoil with different cavitation models based on level set method. Appl Sci 9(4):758

Yuan W, Sauer J, Schnerr GH (2001) Modeling and computation of unsteady cavitation flows in injection nozzles. Mécanique Ind 2(5):383–394

Zahiri A-P, Roohi E (2019) Anisotropic minimum-dissipation (AMD) subgrid-scale model implemented in OpenFOAM: verification and assessment in single-phase and multi-phase flows. Comput Fluids 180:190–205

Zahiri A-P, Roohi E (2021) Assessment of anisotropic minimum-dissipation (AMD) subgrid-scale model: gently-curved backward-facing step flow. Int J Mod Phys C 32(05):2150068

Zhang G, Shi W, Zhang D, Wang C, Zhou L (2016) A hybrid RANS/LES model for simulating time-dependent cloud cavitating flow around a NACA66 hydrofoil. Sci China Technol Sci 59(8):1252–1264

Zhou H, Xiang M, Okolo PN, Wu Z, Bennett GJ, Zhang W (2019) An efficient calibration approach for cavitation model constants based on OpenFOAM platform. J Mar Sci Technol 24(4):1043–1056

Zwart PJ, Gerber AG, Belamri T (2004) "A two-phase flow model for predicting cavitation dynamics," In: Fifth international conference on multiphase flow, Yokohama, Japan, vol. 152